Coverage Probability of EH-enabled LoRa networks - A Deep Learning Approach

Thi-Tuyet-Hai Nguyen[1], Tran Cong Hung[2,*], Nguyen Hong Son[1], Tan Hanh[1], Tran Trung Duy[3], Lam-Thanh Tu[4]

[1]Faculty of Information Technology, Posts and Telecommunications Institute of Technology, Vietnam; ntthai@ptit.edu.vn, sonngh@ptit.edu.vn, tanhanh@ptit.edu.vn

[2]School of Computer Science & Engineering, Saigon International University, Ho Chi Minh City, Vietnam; tranconghung@siu.edu.vn

[3]Faculty of Telecommunications, Posts and Telecommunications Institute of Technology, Vietnam; duytt@ptit.edu.vn

[4]Communication and Signal Processing Research Group, Faculty of Electrical and Electronics Engineering, Ton Duc Thang University, Ho Chi Minh City, Vietnam; tulamthanh@tdtu.edu.vn

Abstract

The performance of energy harvesting (EH)-enabled long-range (LoRa) networks is analyzed in this work. Specifically, we employ deep learning (DL) to estimate the coverage probability (Pcov) of the considered networks. Our study incorporates a general fading distribution, specifically the Nakagami-m distribution, and utilizes tools from stochastic geometry (SG) to model the spatial distributions of all nodes and end-devices (EDs) with EH capability. The DL approach is employed to overcome the limitations of model-based methods that can only evaluate the Pcov under simplified network conditions. Therefore, we propose a deep neural network (DNN) that estimates the Pcov with high accuracy compared to the ground truth values. Additionally, we demonstrate that DL significantly outperforms the Monte Carlo simulation approach in terms of resource consumption, including time and memory.

1. Introduction

Low power wide area networks (LPWAN) have recently been considered the best candidate for implementing the Internet of Things (IoT) compared with cellular networks and WiFi, thanks to their low power consumption and long transmission distances [1, 2]. Among all available LPWAN networks, long-range (LoRa) has gained significant attention from both academia and industry. The success of LoRa networks is attributed to its advanced modulation scheme, chirp spread spectrum (CSS), which provides better performance compared to conventional modulations such as quadrature amplitude modulation (QAM) and

phase shift keying (PSK). Other advantages of LoRa networks include extremely low power consumption and the ability to communicate over distances of up to tens of kilometers by appropriately adjusting the spreading factor (SF), coding rate (CR), and transmit power [3]. Even though LoRa end-devices (EDs) can operate and last for several years, they eventually need to be replaced. This replacement is challenging if the EDs are located in unpopulated areas. Additionally, if the number of EDs is in the tens of thousands, such replacement becomes almost infeasible. As a result, finding solutions to improve energy efficiency (EE) and avoid such maintenance tasks are critically important for LoRa networks.

Luckily, energy harvesting (EH) techniques have been widely studied and employed in the last decade. By charging the devices' batteries with radio frequency

---

*Corresponding author. Email: tranconghung@siu.edu.vn

(RF) signals, one can eliminate the need for battery replacement [4]. The practical implementation of EH in wireless networks includes two approaches. The first approach is to split the RF signals between information decoding and energy harvesting, known as simultaneous wireless information and power transfer (SWIPT) [5]. The second approach is to install power stations to broadcast RF signals to charge the batteries of EDs. It is clear that the latter approach provides better performance as it does not share the RF signals between the energy harvester and information decoder. However, from an economic perspective, the latter approach is more costly than the former.

In wireless communication systems, besides EH technologies and LoRa networks, deep learning (DL) has also been widely applied to solve problems that cannot be addressed via model-based approaches [6–8]. By exploiting the power of data-driven methods, several long-standing problems in wireless networks have been solved. Consequently, in the present work, we address the performance of EH-enabled LoRa networks by employing the DL approach to take advantage of all these advanced technologies and networks.

1.1. Literature review

In this section, we summarize existing works related to the topics of energy harvesting, deep learning in LoRa networks, and the combinations of these techniques. Starting with energy harvesting in wireless networks, this area has been widely studied [9–13]. For instance, Le *et al.* investigated the performance of EH-enabled dual-hop multi-input multi-output (MIMO) systems, deriving the characteristics of the end-to-end (e2e) signal-to-noise ratio (SNR) with two protocols: time switching and power splitting. However, they focused on general wireless systems instead of specific networks such as cellular networks, WiFi, and LPWAN. The work in [10] investigated the performance of the mutual inductance of the transmitter and receiver in wireless power transfer-enabled systems. In contrast, we consider LoRa networks employing deep learning techniques. Huan and other authors in [12] derived the outage probability (OP) of multi-hop relaying networks with energy harvesting and partial relay selection, representing the OP in a closed-form expression. Again, they considered a generic wireless network and did not use deep learning techniques to estimate the performance metric too. User selection protocols, including random selection, distance-based selection, and channel gain based selection, with energy harvesting and hardware impairment, were investigated in [13]. Specifically, they derived the OP under three different selection schemes.

Regarding LoRa networks, Georgiou and his colleagues in [14] derived the coverage probability (Pcov) of LoRa networks. However, they assumed that the signal-to-noise ratio and signal-to-interference ratio (SIR) are independent of each other, whereas we consider this strong correlation in the present work. Thanh and others in [15] also derived the Pcov of LoRa networks, considering the correlation between SIR and SNR, and additionally derived the area spectral efficiency (ASE) of the networks. Nevertheless, they did not incorporate both energy harvesting and deep learning in their work. The performance of multi-gateway downlink LoRa networks was addressed in [16]. Several multiple access methods in LoRa networks were studied in [17], revealing that slotted-ALOHA outperformed the conventional ALOHA approach. The integration of EH-enabled in LoRa networks were deployed in reality. Particularly, Orfei and colleagues, for instance, studied the application of LoRa networks in road monitoring in Rome, Italy, where LoRa devices were powered by energy harvested from electromechanical sources [18]. On the other hand, Dalpiaz *et al.* conducted an experiment using a battery-free power meter in LoRa networks, employing a simple energy harvester circuit using electrical induction and a capacitor [19]. Additionally, authors in [20] utilized EH-enabled LoRa networks to monitor water supply, where the transceiver was powered by a hybrid of solar and hydroelectric sources. Their results demonstrated that with EH-enabled technology, the system's lifetime increased to 432 hours. Another example is from Meli and Bachmann in [21], who reported a solar-powered LoRa system. Their experiments showed that when the transceiver was placed near a window, the LoRa module could transmit hundreds of messages per day. For further practical implementations, demos, and experiments of EH-enabled LoRa and LoRaWAN networks, please refer to [22] and the references therein.

Regarding deep learning in LoRa networks, the authors in [23] applied deep reinforcement learning to enhance the LoRa gateway energy efficiency by optimizing channel and spreading factor allocation. The work in [24] also addressed the energy efficiency of LoRa networks using a DL approach, focusing on system-level EE rather than device-level like [23]. However, these works did not consider energy harvesting in LoRa networks. The combination of LoRa networks and EH was studied in [25], where they derived the steady-state distribution of the capacitor voltage and the outage probability under the impact of co-SF interference. Our previous work in [26] also derived the Pcov of EH-enabled LoRa networks. Nonetheless, neither [25] nor [26] used DL to study and optimize performance of the LoRa networks.

Different from the above-mentioned works, the present study considers EH-enabled LoRa networks and investigates their performance using the DL approach. Additionally, we take into account the correlation

between SIR and SNR, the general fading such as Nakagami-m, and tools from stochastic geometry (SG). Specifically, the primary innovations and contributions of this work are summarized as follows:

- We consider EH-enabled LoRa networks employing stochastic geometry and deep learning. We model the fading with Nakagami-m distribution and the spatial distribution of the end-devices using a homogeneous Poisson point process (HPPP). The correlation between SIR and SNR is also taken into account.

- We design a neural network (NN) to estimate the Pcov performance. Our results show that the well-trained DNN provides highly accurate outcomes, with a mean square error (MSE) and mean absolute error (MAE) of the test set being less than 10^{-4} and 0.004, respectively. The estimated Pcov and the corresponding ground truth values overlap too.

- We unveil several insights from extensive computational results, highlighting the advantages of the DL approach compared to Monte Carlo simulation.

The structure of the manuscript is organized as follows: Section 2 provides the system model, while the deep neural networks (DNN) design is given in Section 3. Section 4 presents numerical computations and discussions. Finally, Section 5 concludes the manuscript.
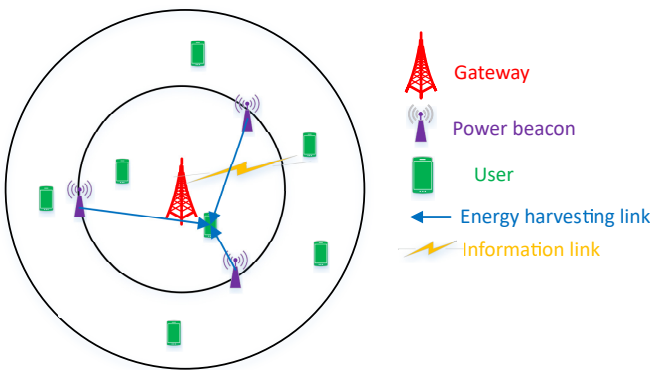
2. System model

Figure 1. The considered EH–based LoRa networks.

Considering a single-gateway uplink LoRa network as shown in Fig. 1. The gateway is located at the center of the disk with radius R, and all LoRa devices are randomly distributed around it. The LoRa end-devices are modeled according to a homogeneous Poisson point process with density Ω. Besides the LoRa gateway

and end-devices, the network also includes M power beacons (PBs) that continuously broadcast wireless signals to charge the EDs' batteries. To maximize the harvested energy, the M power beacons are installed on a circle centered at the network's midpoint. All nodes are equipped with a single antenna. The extension to multiple antennas at the gateway and/or EDs is left for future work. The assumption of the single antenna in LoRa networks is reasonable since LoRa devices are low-cost devices.

2.1. Channel modeling

Let us denote $a_{v,w}$ as the channel coefficient from the transmitter v to the receiver w which is modeled by a Nakagami-m distribution with corresponding shape and spread parameters m and κ. Consequently, the channel gain $a_{v,w}^2$ follows a Gamma distribution with shape and scale parameters m and $\theta = \frac{\kappa}{m}$. The cumulative distribution function (CDF) and probability density function (PDF) of $a_{v,w}^2$, denoted by $F_{a_{v,w}^2}(x)$ and $f_{a_{v,w}^2}(x)$, are computed as follows:

$$F_{a_{v,w}^2}(x) = \frac{1}{\Gamma(m)} \gamma\left(m, \frac{x}{\theta}\right)$$

$$f_{a_{v,w}^2}(x) = \frac{1}{\Gamma(m)\theta^m} x^{m-1} \exp\left(-\frac{x}{\theta}\right), \quad (1)$$

where $\gamma(\cdot, \cdot)$ is the lower incomplete Gamma function, and $\Gamma(\cdot)$ is the Gamma function. Additionally, we further assume that the channel coefficient remains unchanged within one transmission block and changes independently between each transmission.

Remark 1. It should be emphasized that the Nakagami-m distribution is considered a general distribution that can be adapted to other well-known fading models, such as Rayleigh and Rician. Compared with Rayleigh fading, Nakagami-m accounts for the line-of-sight (LOS) component, while Rayleigh fading does not. In comparison with Rician fading, Nakagami-m is more tractable since its probability density function does not involve a special function like the modified Bessel function of the first kind.

Besides the small-scale fading, the signal propagation from transmitter v to receiver w also suffers from large-scale path loss. In the present work, a simplified path-loss model is adopted. Mathematically speaking, the large-scale path-loss from v to w, denoted by $\Delta_{v,w}$, is formulated as

$$\Delta_{v,w} = \Delta_0 (d_{v,w})^\beta, \quad (2)$$

where $\Delta_0 = \left(\frac{4\pi}{\lambda}\right)^2$ is the path-loss constant at the reference distance $d_0 = 1$ meter, $d_{v,w}$ is the distance

between the transmitter v and receiver w, and β is the path-loss exponent. The wavelength, denoted by λ, is given by $\lambda = \frac{c}{f_c}$ where $c = 3 \times 10^8$ m/s is the light speed, and f_c is the carrier frequency in Hz. The path-loss exponent, denoted by β, depends on the transmission environment. For instance, in rural areas, β is close to 2, while in urban environments, β is typically between 3.5 and 4.

2.2. Spreading factor allocation

In the present work, a recently proposed spreading factor allocation based on fair collision (FC) probability is adopted. It is emphasized that the adopted fair collision probability scheme outperforms the conventional distance-based approach as well as random assignment. Under the adopted FC scheme, an end device is assigned the spreading factor c according to the following equation [27]:

$$\text{SF}_c = \frac{\frac{c}{2^c}}{\sum\limits_{b=7}^{12} \frac{b}{2^b}}, \qquad c \in \{7, \ldots, 12\}. \tag{3}$$

2.3. Energy harvesting modeling

All EDs harvest energy from the broadcast signals sent by the power stations. The harvested energy at a generic i-th ED utilizing SF_c, denoted by $E_{i,c}$, is then evaluated as follows:

$$E_{i,c} = T_{har,c}\, \omega \sum_{m=1}^{M} \frac{P_S a_{m,i}^2}{\Delta_{m,i}}, \tag{4}$$

where P_S is the transmit power of the power station; $\omega \in (0, 1)$ is the energy harvesting efficiency; $a_{m,i}^2$ and $\Delta_{m,i}$ are the channel gain and path-loss from the m-th power station to the i-th ED. $T_{\text{har},c}$ is the harvesting duration, which is equivalent to the idle mode of the ED utilizing SF_c, and is computed as follows:

$$T_{har,c} = T_{dur,c} - T_{trans,c},$$
$$T_{dur,c} = \max\left\{ \frac{T_{tx,c}}{\chi}, T_{bet} \right\}. \tag{5}$$

Here, $T_{\text{dur},c}$ is the whole transmission duration of SF_c; $T_{\text{tx},c} = \frac{2^c}{\text{BW}} L_{\text{pac}}$ is the duration of the packet with SF_c where L_{pac} (bytes) is the length of the packet; BW represents the bandwidth of the system; T_{bet} is the duration between two reports of the EDs; χ is the duty cycle and is regulated by the government. Typically, χ should be less than 1%; $T_{\text{trans},c}$ is the transmission duration under spreading factor c. In general, $\frac{T_{\text{tx},c}}{\chi} \ll T_{\text{bet}}$, thus, $T_{\text{har},c}$ can be rewritten as

$$T_{har} \approx T_{bet} - T_{trans}, \ \forall c. \tag{6}$$

2.4. SNR and SIR at the gateway

The signal-to-noise ratio and signal-to-interference ratio at the gateway for a desired ED denoted by 0 using SF_c are formulated as follows:

$$SNR_{0,c} = \frac{P_{0,c} a_0^2}{\Delta_0 \sigma^2},$$

$$SIR_{0,c} = \frac{\frac{P_{0,c} a_0^2}{\Delta_0}}{\sum\limits_{i \in \Omega_c^A} \frac{P_{i,c} a_i^2}{\Delta_i}}, \tag{7}$$

where $P_0 = \frac{E_0}{T_{trans}} = \frac{T_{har}}{T_{trans}} \sum\limits_{m=1}^{M} \frac{P_S a_{m,0}^2}{\Delta_0 d_{m,0}^\beta}$ represents the transmit power of the desired ED. The noise variance at the gateway is given by $\sigma^2 = 10^{-174 + NF + 10 \log_{10}(BW)/10}$. Here, $a_{e,0}^2$ and $d_{e,0}^\beta$, with $e \in \{m, i\}$, denote the small-scale fading and large-scale path-loss from the e-th transmitter to the desired ED. Additionally, $\Omega_c^A = \chi \times \Omega \times \text{SF}_c$ represents the set of active EDs using the same spreading factor as the desired ED.

Remark 2. Direct inspection of (7) reveals the following observations:

- The transmit power of the ED, P_0, is a random variable (RV) rather than a constant number, as assumed in previous works. Specifically, P_0 depends on the channel gain and path-loss from all power beacons to the EDs. Unfortunately, the characteristics of this random variable, including its cumulative distribution function and probability density function, cannot be expressed in closed form for an arbitrary number of PBs or for Rayleigh fading.

- The signal-to-interference ratio and signal-to-noise ratio are strongly correlated because they share the same random variables: P_0, a_0^2, and Δ_0. Additionally, P_0 and P_i are also correlated due to the fixed positions of the PBs, which means the distances from PBs to EDs are correlated.

2.5. Performance metrics

In this work, we use coverage probability as the sole performance metric. In LoRa networks, the coverage probability differs from conventional communications systems. Specifically, Pcov is defined as the joint probability of both the signal-to-noise ratio and signal-to-interference ratio, rather than being expressed in terms of the signal-to-interference-plus-noise ratio (SINR). Mathematically, the coverage probability for the generic end-device using spreading factor c is formulated as

$$P_{\text{cov}}(c) = \Pr\{SIR_c > z_c, SNR_c > \tau_c\}. \tag{8}$$

Here, $\tau \in \{-6, -9, -12, -15, -17.5, -20\}$ (dBm) represents the SNR threshold. The smallest value, $\tau = -20$ dBm, corresponds to spreading factor SF12, and increasing the spreading factor will raise the SNR threshold. Conversely, the largest value, $\tau = -6$ dBm, corresponds to SF7. The term z_c represents the SIR threshold for co-SF interference and is given by $z_c = 1, \forall c$ as stated in [3]. It is important to note that we assume perfect orthogonality between spreading factors, and thus there is no capture effect considered in this work.

As pointed out in Remark 2, both SIR and SNR include many correlated RVs, making it infeasible to find their CDF and PDF. To address the strong correlation between SIR and SNR in (8), some works in the literature approximate this by treating them as two independent probabilities [14, 28], such that $P_{\text{cov}}(c) = \Pr\{SIR_c > z_c, SNR_c > \tau_c\} \approx \Pr\{SNR_c > \tau_c\} \Pr\{SIR_c > z_c\}$. Nevertheless, the CDF and PDF of the SNR and SIR conditions themselves still cannot be expressed in closed-form expressions [28]. Therefore, in this work, we compute the joint probability in (8) by leveraging the power of data-driven approach, specifically the deep learning. We propose and design a deep neural network to estimate the Pcov of the considered networks. The design of the proposed DNN is provided in the next section.

3. Deep neural networks design
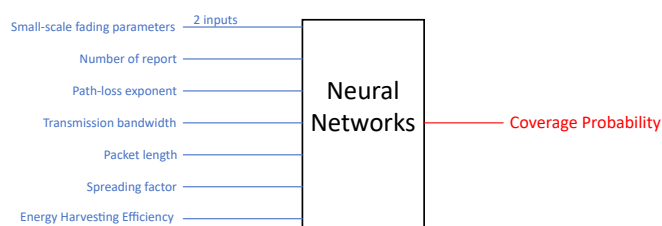
3.1. Dataset creation

Figure 2. Deep neural networks.

It is evident that training any neural network is impossible if the dataset is missing. However, since the considered network is novel, real-world data is unavailable. Consequently, synthetic data is generated using the Monte-Carlo method. Each sample includes one output, i.e., coverage probability, and eight inputs: path-loss exponent, shape and scale parameters of the Nakagami-m fading, transmission bandwidth, packet length, number of reports per day, energy efficiency conversion, and transmit power of the power beacon. Fig. 2 illustrates the input-output relationship of the NN. It is noted that the data range aligns with LoRa standardization and covers a wide range

of transmission environments. The entire dataset is divided into three parts: 70% for the training set, 20% for the development set, and the remaining 10% for the test set.

3.2. Normalization

All data samples are normalized using max-min normalization. Mathematically, the input and output of the normalization process are given by

$$w_o = \frac{w_i - \min(w_i)}{\max(w_i) - \min(w_i)}, \tag{9}$$

where w_i and w_o denote the input and output of the normalization, respectively, and $\max(\cdot)$ and $\min(\cdot)$ are the maximum and minimum functions. From (9), we observe that w_o ranges between zero and one.

3.3. Hyper parameters selection

The hyperparameters are carefully designed and selected to optimize the DNN performance. Specifically, the number of hidden layers and the number of neurons per layer are optimized using the grid search approach. For simplicity, we consider an architecture where all hidden layers have the same number of neurons, denoted by $\mathcal{L}$ layers and $\mathcal{N}$ neurons, denoted by the shorthand $(\mathcal{L}, \mathcal{N})$. For the optimizer, we use the widely-adopted Adam optimization approach [29].

3.4. Loss function

All training processes require at least one loss function to minimize, and in this work, we use the mean square error as the loss function for the neural network. Specifically, it is formulated as follows:

$$\min \text{MSE} = \frac{1}{\|\Upsilon_{\text{train}}\|} \sum_{y \in \Upsilon_{\text{train}}} \left(q_y - \widetilde{q}_y\right)^2, \tag{10}$$

where Υ_X, $X \in \{\text{train, devel, test}\}$, represents the X-th dataset; $\|\cdot\|$ denotes the cardinality of the set Υ; and q_y and $\widetilde{q}_y$ are the ground truth value and its estimated version, respectively.

3.5. Performance metric of the neural networks

Apart from the MSE, we also adopt another metric to evaluate the performance of the NN. More precisely, we use the mean absolute error and is formulated as follows:

$$\text{MAE} = \frac{1}{\|\Upsilon_X\|} \sum_{y \in \Upsilon_X} \left|q_y - \widetilde{q}_y\right|. \tag{11}$$

4. Numerical computations and discussions

In this section, we present numerical results to verify the accuracy of the estimated coverage probability against the ground truth values. We also provide the mean square error and mean absolute error for the deep neural network on the training set, development set, and test set. All parameters used for the numerical computations are listed in Table 1, while the architecture of the DNN is detailed in Table 2.

Table 1. Numerical Parameters [26].

Parameters	Value
Spreading factor	$\{7, 8, 9, 10, 11, 12\}$
Duty cycle	$\chi = 0.1\%$
Carrier frequency	$f_c = 920$ MHz
Noise figure	NF = 6 dBm
SNR threshold	$z \in \{-6, -9, -12, -15, -17.5, -20\}$ dBm
Path-loss exponent	$\beta \in [2.5, 4]$
Packet length	$L_{pac} \in [10, 200]$ bytes
Transmission bandwidth	$\beta \in \{125, 250\}$ kHz
Power beacon transmit power	$P_S \in [0, 60]$ dBm
Energy conversion efficiency	$\omega \in (0, 1)$
Number of report per day	$N_{report} \in \{0.5, 1 : 24, 48, 96, 144, 288\}$
Shape parameter	$m \in [0.5, 10]$
Scale parameter	$\theta \in [0.01, 10]$
Network radius	$R = 1.5$ km
Number of power beacon	$M = 10$
Density of EDs	$\Omega = \frac{\bar{N}_{ED}}{\pi R^2} = 1.414 \times 10^{-4}$ ED/m^2
SIR threshold	$\tau_c = \tau = 1, \forall c$
Transmission duration	$T_{trans} = 3$ sec

Fig. 3 illustrates the mean square error of the training set with respect to the number of epochs for different DNN architectures. We observe that the MSE monotonically decreases as the number of epochs

---

[1]It is evident that a larger training set typically leads to better results. However, in this section, a training set of 14000 samples is used for training the DNN, as it already yields reasonably good results, as depicted in Figs. 5, 6, and 7. However, in future work, additional samples will be included to further improve the system's performance.

Table 2. The DNN architecture (Unless otherwise stated)

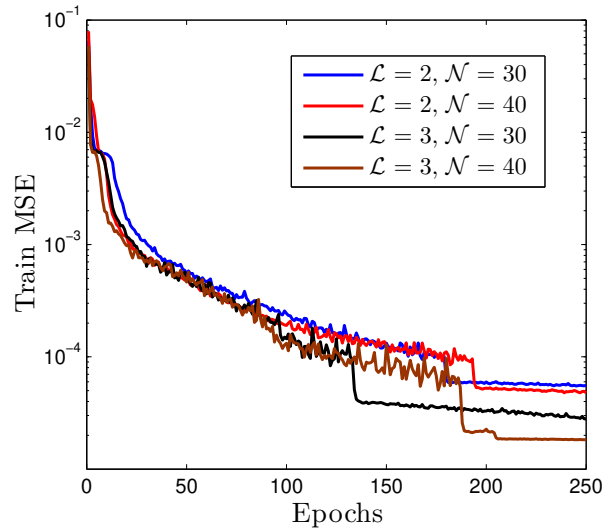| Parameters	Value
Epochs	250
Number of input	8
Number of output	1
Number of hidden layers	$\mathcal{L} = 3$
Number of neurons per layer	$\mathcal{N} = 40$
Size of training set	$\|\Upsilon_{\text{train}}\| = 14000$[1]
Size of development set	$\|\Upsilon_{\text{dev}}\| = 4000$
Size of test set	$\|\Upsilon_{\text{test}}\| = 2000$

Figure 3. Training MSE versus number of epochs with different hidden layers and number of neurons per layer

increases, with all settings becoming almost stable from 200 epochs onward. Thus, unless otherwise stated, 250 epochs are used to train the neural networks in this section. From Fig. 3, we also observe that the setup with $\mathcal{L} = 3$ layers and $\mathcal{N} = 40$ neurons, i.e., $(3, 40)$, outperforms other configurations starting from the 200th epoch. Consequently, we use the setup $(3, 40)$ for the entire section unless specifically stated otherwise. Conversely, the $(2, 30)$ configuration yields the worst results, while the $(3, 30)$ and $(2, 40)$ setups rank 2nd and 3rd, respectively. Additionally, we see that all architectures exhibit similar performance when the number of epochs is less than 120.

The MSE performance of the development set with respect to the number of epochs is provided in Fig. 4.
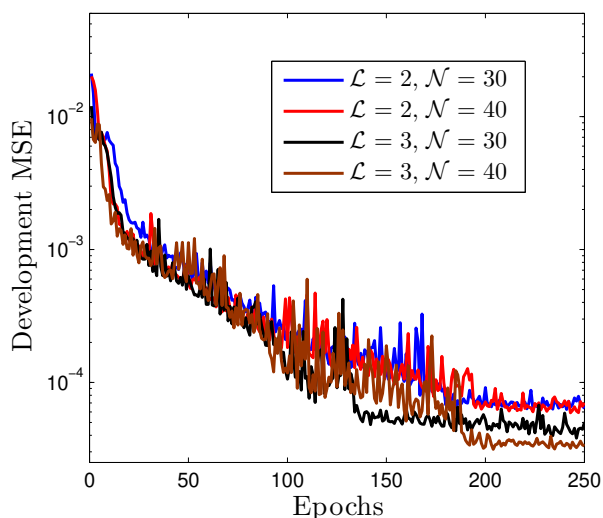
Figure 4. Development MSE versus number of epochs with different hidden layers and number of neurons per layer

Table 3. Computation time for each sample

Method	Times (seconds)
Monte-Carlo simulation	≈ 16
DNN	< 1

Similar to the observations from Fig. 3, the architecture $(3, 40)$ provides the best performance out of all settings. Additionally, the performance of the development set and the training set are quite similar, with the best performance reaching approximately 4×10^{-5}.

The MSE performance of the best epoch for all configurations is shown in Fig. 5 for both the training and development sets. We observe that the $(3, 40)$ configuration consistently outperforms the other setups. Interestingly, with the exception of the $(2, 10)$ setup—where the development MSE is better than the training MSE—all other configurations display the opposite trend, with the training set MSE consistently outperforming the development set MSE. For $\mathcal{L} = 2$, the MSE continues to improve up to approximately 20 neurons per layer. This is likely because a minimal number of neurons does not allow the system to learn effectively, and increasing the neuron count initially improves performance. However, further increases in neuron count in a two-layer network provide diminishing returns, as the network approaches its capacity limits, with MSE plateauing around 5×10^{-5}. For $\mathcal{L} = 3$, the MSE continues to decrease until $\mathcal{N} = 40$, beyond which it starts to increase, indicating that the $(3, 40)$ configuration is optimal for the considered networks.

Fig. 6 illustrates the MAE of the development set using the best epoch for each configuration. Generally, we observe the same trend as with the MSE, increasing the number of neurons $\mathcal{N}$ within the same number of layers $\mathcal{L}$ is beneficial. This figure also reveals that even the worst setup, $(2, 10)$, has an MAE below 8×10^{-3}. This level of accuracy is acceptable for

most applications, such as evaluating the coverage probability. Additionally, the best setup, $(3, 40)$, is only about twice as accurate as the worst setup, demonstrating that even the less optimal configurations perform reasonably well.

The MSE and MAE of the test set from the best epoch of the development set are shown in Fig. 7. We observe that the performance of both MSE and MAE is slightly worse compared to the training and development sets. Nonetheless, the performance remains within an acceptable range. For instance, the MSE of the setting $(3, 40)$ is less than 10^{-4}, while the MAE is below 0.004.

Table 3 illustrates the computation time required for estimating the Pcov using both the Monte-Carlo and DNN approaches. It is evident that the DNN significantly outperforms the Monte-Carlo approach under the current setup, providing faster estimation times. Additionally, the Monte-Carlo simulation consumes more memory than the DL approach provided that the DNN is well-trained.

Fig. 8 shows the Pcov for both the estimated and ground truth versions. We observe that the estimated curve and the ground truth curve perfectly overlap, demonstrating that a well-trained DNN can estimate the Pcov with very high accuracy.

Fig. 9 studies the impact of the number of hidden layers on the performance of the MAE under the test set. We observe that the MAE increases beyond $\mathcal{L} = 3$, suggesting that $\mathcal{L} = 3$ is optimal for the considered networks. This aligns with the universal approximation theorem, which states that deeper networks generally capture more complex features. However, as shown in Fig. 9, further increasing the number of layers leads to overfitting, causing the DNN's performance to decline.

5. Conclusion

The performance of the EH-enabled LoRa networks was addressed in the present work. By leveraging deep learning, we were able to estimate the Pcov with very high accuracy, overcoming the limitations of the model-based approach that only computes for simple networks. Compared with the Monte Carlo approach, the deep learning approach consumes fewer resources, provided the neural network is well-trained. There are several ways to enhance the contributions of the present work. An immediate extension of this
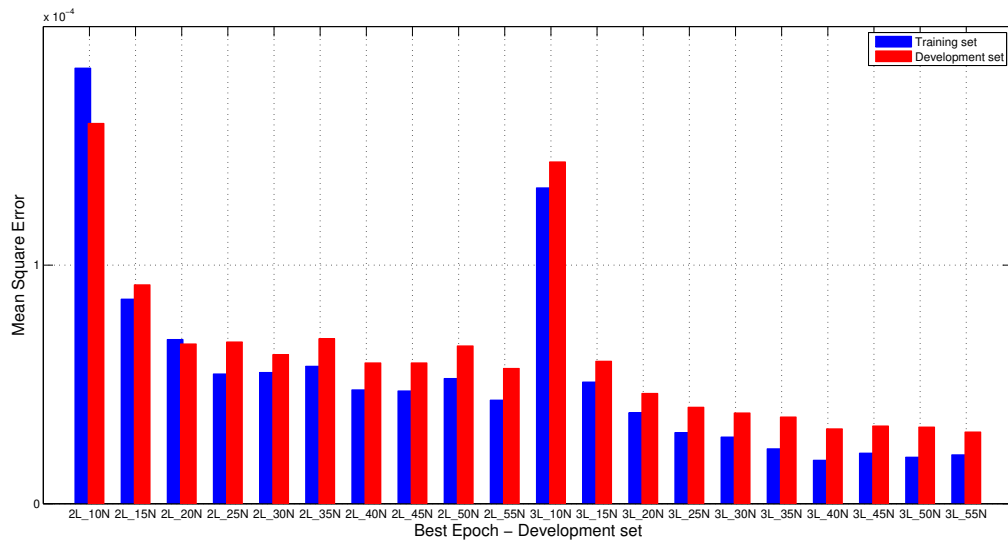
Figure 5. MSE versus best epochs of both training and development set with different hidden layers and number of neurons per layer
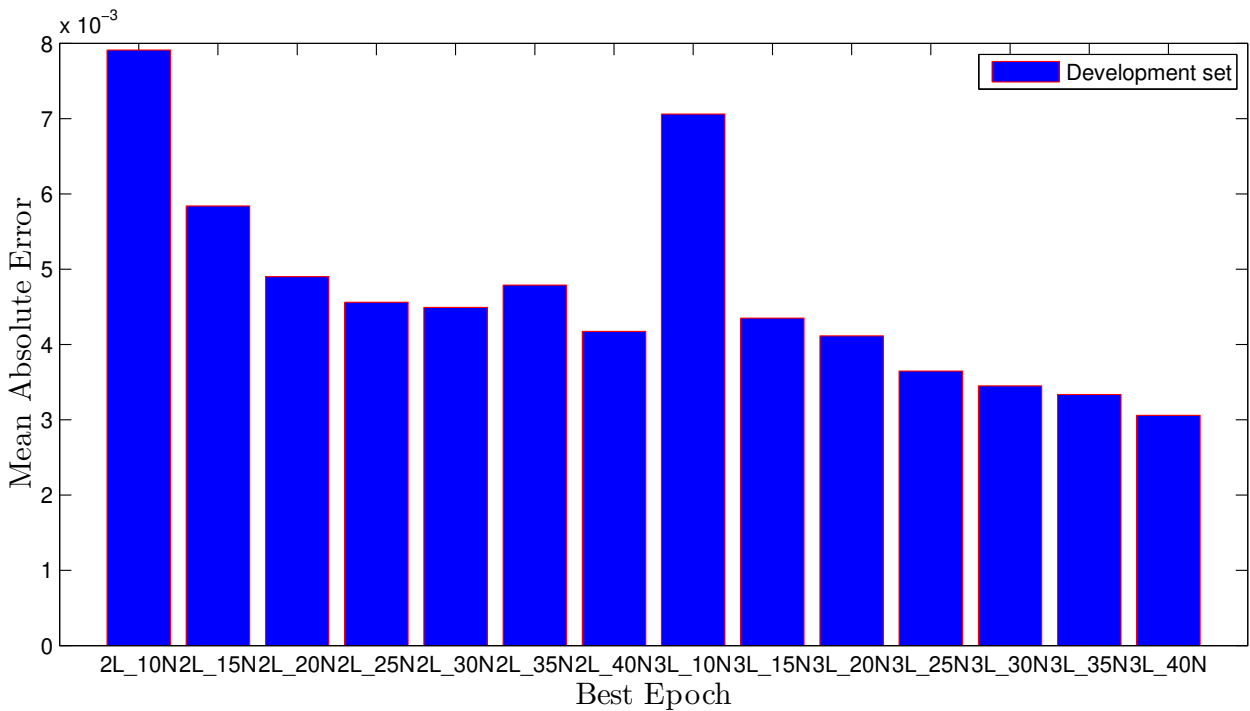

Figure 6. MAE versus best epochs of development set with different hidden layers and number of neurons per layer.

work could be to maximize the coverage probability by optimizing key parameters such as LoRa device transmit power, transmission bandwidth, and packet length. One promising method is to use Fountain codes to significantly enhance the spectral efficiency of the networks [30]. Another possible direction is to consider multi-hop relaying networks to shorten the transmission distance and save transmit power, thus improving both spectral efficiency and energy efficiency [31].
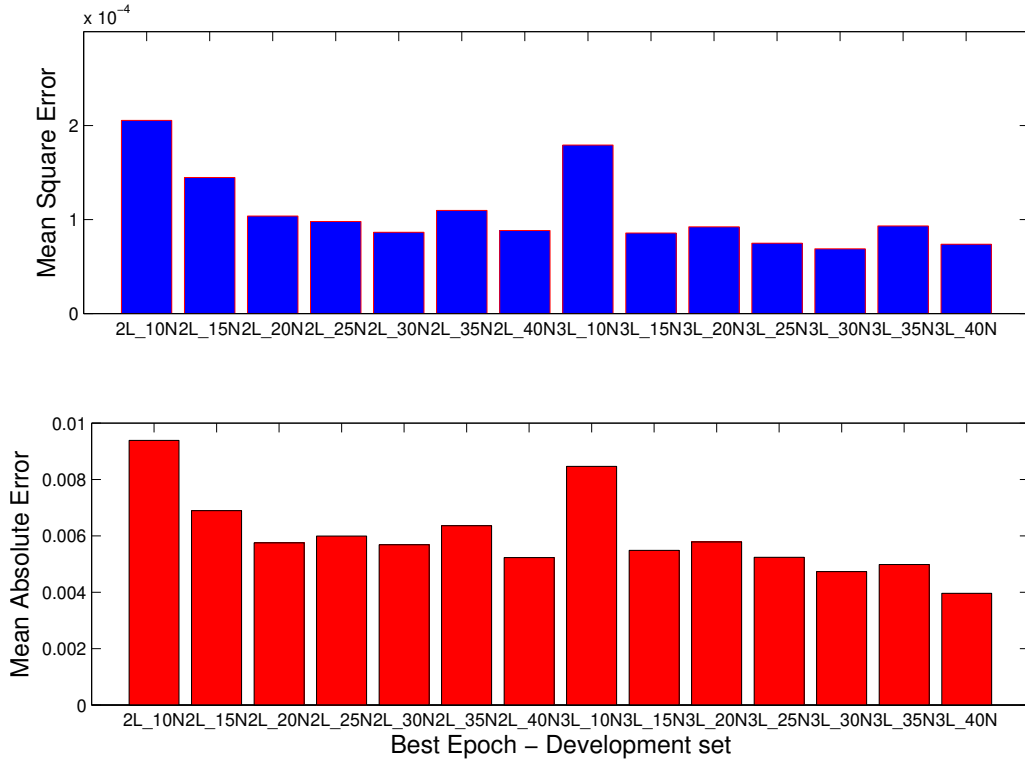
Figure 7. MAE and MSE versus best epoch of development set on the test set with different hidden layers and number of neurons per layer.
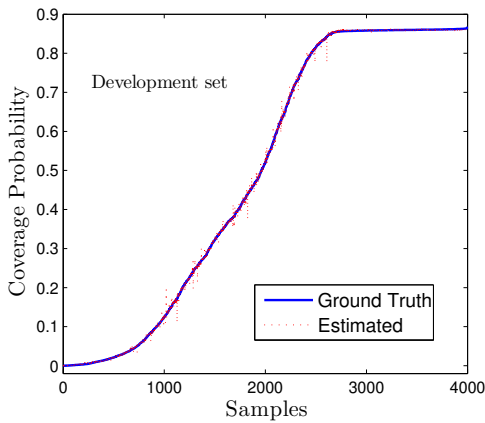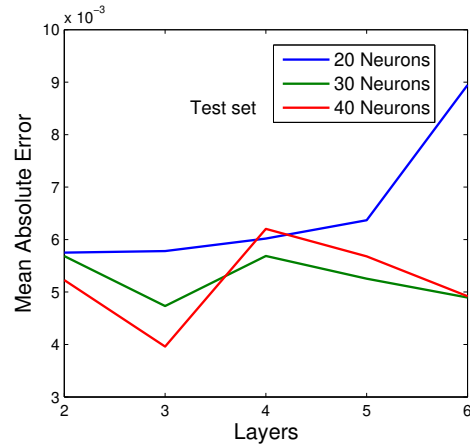

Figure 8. Pcov vs. samples in the increasing order.

Figure 9. MAE vs. number of hidden layers, $\mathcal{L}$, of the test set with various number of neurons per layer.

References

[1] GOURSAUD, C. and GORCE, J.M. (2015) Dedicated networks for IoT: PHY / MAC state of the art and challenges. *EAI Endorsed Transactions on Internet of Things* **1**(1): 150597. doi:10.4108/eai.26-10-2015.150597, URL

https://doi.org/10.4108/eai.26-10-2015.150597.

[2] RAZA, U., KULKARNI, P. and SOORIYABANDARA, M. (2017) Low power wide area networks: An overview. *IEEE Communications Surveys and Tutorials* **19**(2): 855–873. doi:10.1109/COMST.2017.2652320.

[3] TU, L.T., BRADAI, A., POUSSET, Y. and ARAVANIS, A.I. (2022) On the spectral efficiency of lora networks: Performance analysis, trends and optimal points of operation. *IEEE Transactions on Communications* **70**(4): 2788–2804. doi:10.1109/TCOMM.2022.3148784.

[4] HOANG, T.M., DUONG, T.Q., VO, N.S. and KUNDU, C. (2017) Physical layer security in cooperative energy harvesting networks with a friendly jammer. *IEEE Wireless Communications Letters* **6**(2): 174–177. doi:10.1109/LWC.2017.2650224.

[5] NASIR, A.A., ZHOU, X., DURRANI, S. and KENNEDY, R.A. (2013) Relaying protocols for wireless energy harvesting and information processing. *IEEE Transactions on Wireless Communications* **12**(7): 3622–3636. doi:10.1109/TWC.2013.062413.122042.

[6] SAIKIA, P., SINGH, K., HUANG, W.J. and DUONG, T.Q. (2024) Hybrid deep reinforcement learning for enhancing localization and communication efficiency in ris-aided cooperative isac systems. *IEEE Internet of Things Journal* : 1–1doi:10.1109/JIOT.2024.3411158.

[7] ANSERE, J.A., GYAMFI, E., SHARMA, V., SHIN, H., DOBRE, O.A. and DUONG, T.Q. (2024) Quantum deep reinforcement learning for dynamic resource allocation in mobile edge computing-based iot systems. *IEEE Transactions on Wireless Communications* **23**(6): 6221–6233. doi:10.1109/TWC.2023.3330868.

[8] HAZARIKA, B., SINGH, K., PAUL, A. and DUONG, T.Q. (2024) Hybrid machine learning approach for resource allocation of digital twin in uav-aided internet-of-vehicles networks. *IEEE Transactions on Intelligent Vehicles* **9**(1): 2923–2939. doi:10.1109/TIV.2023.3335277.

[9] LE, N.P., VO, N.S., HOANG, M.T. and TRAN, D.D. (2017) Unified analysis of energy harvesting–based mimo relay wireless systems over nakagami-m fading channels. *Transactions on Emerging Telecommunications Technologies* **28**(10): e3160. doi:https://doi.org/10.1002/ett.3160, URL https://onlinelibrary.wiley.com/doi/abs/10.1002/ett.3160. E3160 ett.3160, https://onlinelibrary.wiley.com/doi/pdf/10.1002/ett.3160.

[10] ZHENG, J. (2023) Analysis of mutual inductance between transmitter and receiver coils in wireless power transfer system of electric vehicle. *Advances in Electrical and Electronic Engineering* **21**(3). doi:10.15598/aeee.v21i3.4991, URL http://dx.doi.org/10.15598/aeee.v21i3.4991.

[11] ROY, J.S. and MISHRA, S.S. (2023) Sc-fdma uplink system in heavily faded areas with low signal-to-noise ratio. *Advances in Electrical and Electronic Engineering* **21**(3). doi:10.15598/aeee.v21i3.4987, URL http://dx.doi.org/10.15598/aeee.v21i3.4987.

[12] HUAN, N.T., DUY, T.T., TU, L.T., SANG, N.Q., TA, Q.H. and TUAN, P.V. (2022) Incremental cooperation based multi-hop relaying scheme with fountain codes, wirelessly energy harvesting and partial relay selection. In *2022 International Conference on Advanced Technologies for Communications (ATC)*: 338–343. doi:10.1109/ATC55345.2022.9943044.

[13] NGUYEN, T.N., DUY, T.T., TRAN, P.T. and VOZNAK, M. (2016) Performance evaluation of user selection protocols in random networks with energy harvesting and hardware impairments. *Advances in Electrical and Electronic Engineering* **14**(4). doi:10.15598/aeee.v14i4.1783, URL https://doi.org/10.15598/aeee.v14i4.1783.

[14] GEORGIOU, O. and RAZA, U. (2017) Low power wide area network analysis: Can lora scale? *IEEE Wireless Communications Letters* **6**(2): 162–165. doi:10.1109/LWC.2016.2647247.

[15] TU, L.T., BRADAI, A. and POUSSET, Y. (2020) A new closed-form expression of the coverage probability for different qos in lora networks. In *ICC 2020 - 2020 IEEE International Conference on Communications (ICC)*: 1–6. doi:10.1109/ICC40277.2020.9148720.

[16] TU, L.T., BRADAI, A. and POUSSET, Y. (2022) Coverage probability and spectral efficiency analysis of multi-gateway downlink lora networks. In *ICC 2022 - IEEE International Conference on Communications*: 1–6. doi:10.1109/ICC45855.2022.9838363.

[17] BELTRAMELLI, L., MAHMOOD, A., ÖSTERBERG, P. and GIDLUND, M. (2021) Lora beyond aloha: An investigation of alternative random access protocols. *IEEE Transactions on Industrial Informatics* **17**(5): 3544–3554. doi:10.1109/TII.2020.2977046.

[18] ORFEI, FRANCESCO AND BENEDETTA MEZZETTI, CHIARA AND COTTONE, FRANCESCO (2016) Vibrations powered lora sensor: An electromechanical energy harvester working on a real bridge. In *2016 IEEE SENSORS* (IEEE). doi:10.1109/icsens.2016.7808752, URL http://dx.doi.org/10.1109/ICSENS.2016.7808752.

[19] DALPIAZ, G., LONGO, A., NARDELLO, M., PASSERONE, R. and BRUNELLO, D. (2018) A battery-free non-intrusive power meter for low-cost energy monitoring. In *2018 IEEE Industrial Cyber-Physical Systems (ICPS)* (IEEE): 653–658. doi:10.1109/icphys.2018.8390784, URL http://dx.doi.org/10.1109/ICPHYS.2018.8390784.

[20] BATHRE, M. and DAS, P.K. (2022) Water supply monitoring system with self-powered lora based wireless sensor system powered by solar and hydroelectric energy harvester. *Computer Standards & Interfaces* **82**: 103630. doi:10.1016/j.csi.2022.103630, URL http://dx.doi.org/10.1016/j.csi.2022.103630.

[21] M. MELI, P.B. (2016) Powering long range wireless nodes with harvested energy. In *Wireless Congress 2016: Systems & Applications* (Wireless Congress). URL https://digitalcollection.zhaw.ch/handle/11475/7041.

[22] DELGADO, CARMEN AND SANZ, JOSÉ MARÍA AND BLONDIA, CHRIS AND FAMAEY, JEROEN (2021) Batteryless lorawan communications using energy harvesting: Modeling and characterization. *IEEE Internet of Things Journal* **8**(4): 2694–2711. doi:10.1109/JIOT.2020.3019140.

[23] HAMDI, R., BACCOUR, E., ERBAD, A., QARAQE, M. and HAMDI, M. (2022) Lora-rl: Deep reinforcement learning for resource management in hybrid energy lora wireless networks. *IEEE Internet of Things Journal* **9**(9): 6458–6476. doi:10.1109/JIOT.2021.3110996.

[24] TU, L.T., BRADAI, A., AHMED, O.B., GARG, S., POUSSET, Y. and KADDOUM, G. (2022) Energy efficiency optimization

in lora networks—a deep learning approach. *IEEE Transactions on Intelligent Transportation Systems* : 1–13doi:10.1109/TITS.2022.3183073.

[25] GEORGIOU, O., PSOMAS, C., DEMARCHOU, E. and KRIKIDIS, I. (2021) Lora network performance under ambient energy harvesting and random transmission schemes. In *ICC 2021 - IEEE International Conference on Communications*: 1–6. doi:10.1109/ICC42927.2021.9500756.

[26] NGUYEN, T.T.H., NGUYEN, T.N., DUY, T.T., SON, N.H., HANH, T., VU, M.B. and TU, L.T. (2024) Coverage probability of energy harvesting enabled lora networks with stochastic geometry. *Journal of Information and Telecommunication* **8**(2): 262–279. doi:10.1080/24751839.2023.2281144.

[27] REYNDERS, B., MEERT, W. and POLLIN, S. (2017) Power and spreading factor control in low power wide area networks. In *2017 IEEE International Conference on Communications (ICC)*: 1–6. doi:10.1109/ICC.2017.7996380.

[28] NGUYEN, T.H., JUNG, W.S., TU, L.T., CHIEN, T.V., YOO, D. and RO, S. (2020) Performance analysis and optimization of the coverage probability in dual hop lora networks with different fading channels. *IEEE Access* **8**: 107087–107102. doi:10.1109/ACCESS.2020.3000600.

[29] KINGMA, D.P. and BA, J. (2017), Adam: A method for stochastic optimization. URL https://arxiv.org/abs/1412.6980. 1412.6980.

[30] NGUYEN, Q.S., NGUYEN, V.H., TRAN, T.D., NGUYEN, L.N. and TU, L.T. (2023) On the security and reliability trade-off of the satellite terrestrial networks with fountain codes and friendly jamming. *EAI Endorsed Trans. Industrial Netw. Intel. Sys.* **10**(4). doi:10.4108/eetinis.v10i4.4192.

[31] NAM, P.M., DINH, P.N., NHAT, N.L., LAM-THANH, T. and LE-TIEN, T. (2024) On the performance of the relay selection in multi-hop cluster-based wireless networks with multiple eavesdroppers under equally correlated rayleigh fading. *EAI Endorsed Transactions on Industrial Networks and Intelligent Systems* **11**(3). doi:10.4108/eetinis.v11i3.4728.